Journal of Visualization, Vol. 3, No. 1 (2000) 79-92

Evaluation of Shear and Recirculation in Centrifugal Artificial Heart by Flow Visualization

Asztalos, B.*[1], Yamane, T.*[1], Nishida, M.*[1], Masuzawa, T.*[2] and Konishi, Y.*[3]

*1 Mechanical Engineering Laboratory, 1-2 Namiki, Tsukuba, Ibaraki, 305-8564, Japan.
e-mail: yamane@mel.go.jp
*2 Ibaraki University, Ibaraki, Japan.
*3 Nikkiso Co., Ltd., Tokyo, Japan.

Received 11 June 1999.
Revised 22 October 1999.

***Abstract*:** A centrifugal blood pump for artificial heart has to have low hemolysis and no thrombus formation. For finding and removing the fluid dynamic causes of the above mentioned phenomena, flow visualization was utilized, as flow visualization can identify the high shear and stagnation locations which relate to hemolysis and thrombus formation respectively. In the present paper, general fluid dynamic characteristics of centrifugal blood pumps will be extracted, through analyzing four typical centrifugal pumps with flow visualization technique. Finding shear in the volute and diffuser regions, confirming vortex formation at washout holes, and quantitative analysis of the flow in the inlet regions are the shown examples. The obtained results correspond well to hemolysis tests, which proves that flow visualization is a useful tool in developing and analyzing blood pumps for artificial hearts.

***Keywords*:** flow visualization, particle tracking velocimetry, centrifugal blood pump, shear evaluation, artificial heart

***Index*:** Evaluation of shear and recirculation in artificial heart

1. Introduction

Implantable artificial heart is in high demand by medical doctors for home care nowadays. Small blood pumps are also needed on hospital beds for short-term circulatory support. To satisfy this need for small pumps, centrifugal pumps were found to be suitable for pump size reduction.

These newly developed blood pumps for artificial heart or for heart surgery should be evaluated before clinical use by pump performance test, durability test, hemolysis (blood cell destruction) test, thrombogenic (blood clotting) test with animals, etc. Blood flow behavior should be clarified by hemolysis and thrombogenic tests.

Large number of hemolysis tests are often conducted at the development stage due to the individuality of the used animal blood. Though hemolysis tests give an overall evaluation of a pump, locations where actual hemolysis occurs cannot be specified by this method.

Hemolysis is mainly a mechanical trauma by shear stress inside the pumps. The high shear areas can be identified and measured by flow visualization analysis. Also the investigation of dynamic flow behavior can allow to locating areas of stagnant regions which might be the major sources of thrombus formation.

Centrifugal blood pumps for artificial heart should be small for implantation. The necessary pressure of 13.3 kPa (100 mmHg) can be achieved with impeller tip velocity of 4-7 m/s. At present, the investigated models

operate in the 1900-2700 rpm range to attain a pressure of 13.3 kPa at a flow rate of 5L/min ($8.33 \times 10^{-5} m^3/s$). The mentioned rotational speed was too high even for a high speed video camera of 4500 frames/sec to obtain suitable images for particle tracking velocimetry. Based on the Reynolds similarity law, scale-up models enabled to reduce rotational speed and flow visualization analysis was carried out on these scaled-up models.

We have successfully applied flow visualization for enhancing pump design (Yamane et al.,1997/1), and could reduce the number of necessary hemolysis tests (Yamane et al.,1998) which fastened the design process. In this paper we present our methodology as some applications. We cover the experiment setup, the PTV (Particle Tracing Velocimetry) analysis method, the developed post-processing system, methods for error reduction, a comparison between qualitative and quantitative results, analysis of shear profile and recirculation by utilizing a variety of blood pumps.

2. Experimental Method

2.1 Pump Designs

All investigated pump models are of centrifugal type. Model 1 was a prototype for investigating the function of washout holes on a semi-open impeller which creates a high lifting force (lift reduction by the washout holes). Model 2 is a closed-type impeller model for analyzing the flow around the vanes and in the gaps around the impeller. Model 3 and 4 were used to analyze the effects of the size of the impeller/radial gap. These two models were of the semi-open type also.

Regarding the actual pumps for Model 1 and 2 (Yamane et al., 1995 and 1997/2), they featured an impeller being sustained with a pivot and a magnetic bearing. Model 3 and 4 represent a blood pump for heart surgery (HPM-15, Nikkiso Co.Ltd., Tokyo). Their pictures are shown in Fig.1 and the design parameters are shown in Table 1. All investigated impellers have washout holes placed at each vane to improve flow around the center.

Table 1. Pump geometry (actual size models)

	Model 1 (Prototype)	Model 2 (DD1)	Model 3 (standard gap)	Model 4 (small radial gap)
Impeller type	semi-open	closed	semi-open	semi-open
Impeller diameter	50 mm	50 mm	50 mm	50 mm
Number of vanes	4	4	6	6
Number of washout holes	4	4	6	6
Radial gap (between casing and impeller)	7 mm	1.75-5.15 mm	3 mm	0.5 mm

2.2 Scaled-up Models

Blood pumps rotate at 2000-3000 rpm. This speed is too high for PTV. Therefore speed reduction by scaling-up the pump model is necessary based on Reynolds similarity law. Reynolds number is $Re=UL/\nu$, where U, L and ν are flow velocity, representative length and kinematic viscosity respectively. Keeping Reynolds similarity can be achieved by adjusting the rotational speed. Moreover, to keep the ratio of the tangential and radial velocity constant, the ratio of the flow rate to rotational speed should coincide. This can be achieved by adjusting the valve resistance. This means that it is possible to investigate the flow in a pump by using a different scale model with different fluid. For our experiments the Reynolds number was in the 60000 range.

All scale-up models were made of acrylic resin (refractive index of 1.49), to accommodate visual information gathering. The pump was embedded into an acrylic box, with flat surfaces, and the camera was always placed in a perpendicular position to these surfaces. Model 1 and 2 were made of 3 times scaling while Model 3 and 4 were made of 2.5 times scaling. The scale-up models can be seen on Fig. 2.

2.3 Experimental Setup and Tracer Particles

The experimental setup can be seen on Fig. 3. It consisted of a scale-up model/driving unit and an external circuit of a reservoir and a valve. Pump rotational speed, flow rate and two pressures were measured. Table 2 summarizes the rotational speed/flow rate conditions for the performed experiments.

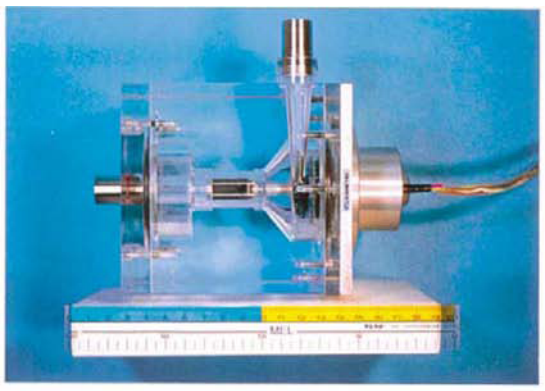

(a)

(b)

(c)

Fig. 1. Actual size pump models : (a) Model 1 (Prototype) ; (b) Model 2 (DD1) ; (c) Model 3&4 (Nikkiso).

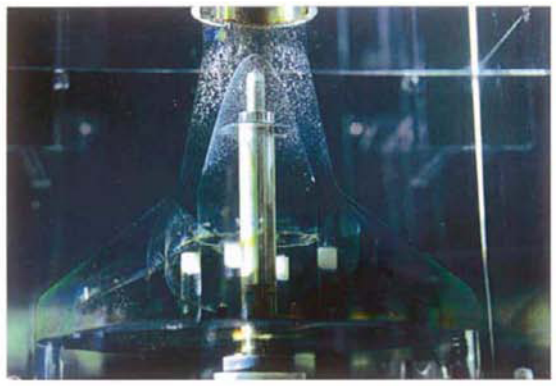

(a)

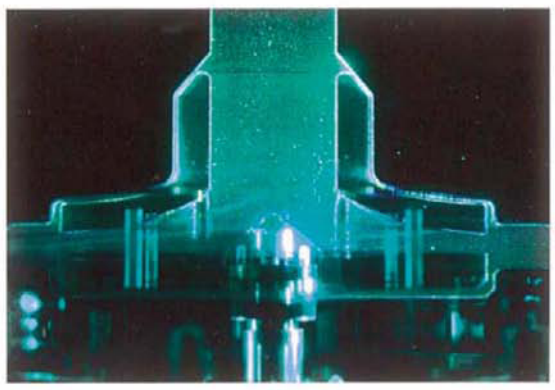

(b)

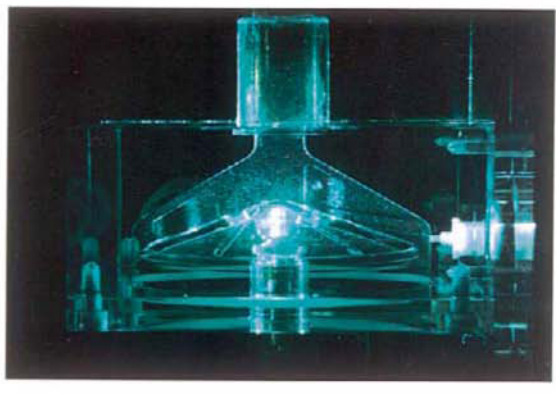

(c)

Fig. 2. Scaled up models : (a) Model 1 (Prototype), ×3 ; (b) Model 2 (DD1), ×3 ; (c) Model 3&4 (Nikkiso), ×2.5.

Table 2. Experimental conditions. Model 3 & 4 have two conditions, as a large pump head was selected in the comparison experiment, corresponding to high hemoly sis condition.

	Model 1 (Prototype)	Model 2 (DD1)	Model 3 (standard gap)		Model 4 (small gap)	
Scale-up rate	3×	3×	2.5×		2.5×	
Rotational speed	180 rpm	126 rpm	183 rpm	259 rpm	183 rpm	259 rpm
Flow rate	9 L/min	9 L/min	7.5 L/min	7.5 L/min	7.5 L/min	7.5 L/min
Equivalent head for actual size model	100 mmHg	100 mmHg	100 mmHg	213 mmHg	100 mmHg	213 mmHg
Equivalent rotational speed for actual size model	2700 rpm	1900 rpm	1900 rpm	2690 rpm	1900 rpm	2690 rpm
Equivalent flow rate for actual size model	5 L/min	5 L/min	5 L/min	5 L/min	5 L/min	5 L/min

(a)

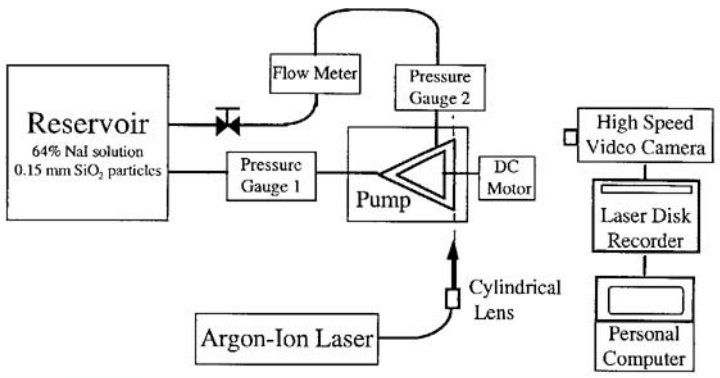

(b)

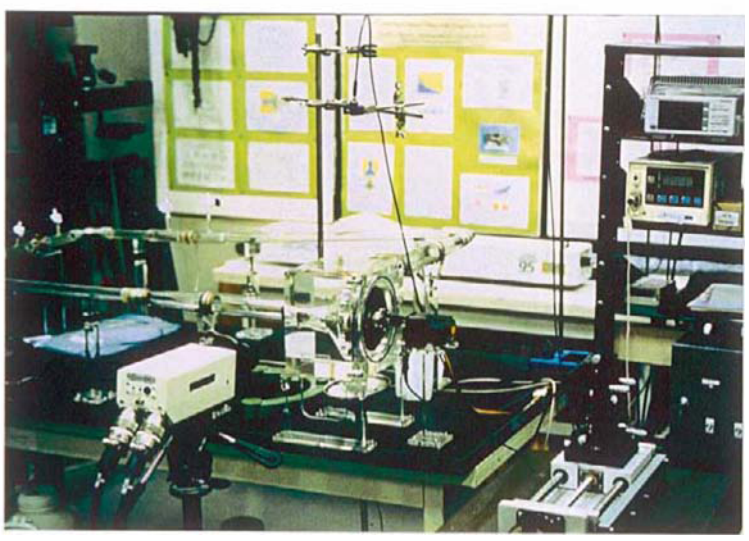

Fig. 3. Experimental setup : (a) Schematic drawing; (b) Photo.

64wt% NaI water solution was selected as working fluid with 0.1wt% $Na_2S_2O_3$ as stabilizer. Since this water solution had exactly the same refractive index (1.49) as the used acrylic resin used for the pump models, one can expect no distortion inside the pump. The solution had a specific gravity of 1.9, and kinematic viscosity of $1.8\times10^{-6}m^2/s$. Typical human blood has a kinematic viscosity of $3\times10^{-6}m^2/s$. Depending on the scaling (3 or 2.5 times) of the models, a speed reduction (1/15 or 1/10.4) could be achieved. Spherical SiO_2 particles (MSF-1500M, Liquid Gas, Osaka, Japan) with a diameter of 150μm and a specific gravity 2.1 were added as tracer particles. As the specific gravity of the tracer particles was close to that of the working fluid (1.9) and the particle diameter was as small as 0.15mm, we could make sure that the particles did not precipitate in still liquid even over 10 minutes. Particles kept their reflective characteristics for approximately 30 minutes, and then their brilliance was deteriorated. For keeping the quality of the obtained images it was necessary to re-seed particles. This deterioration may be caused by the change of particle surface properties in the NaI_{aq} solution. A typical video image can be seen on Fig. 4.

Filling up the circuit, one had to remove the small air bubbles. This was done by a small plastic guide placed in the reservoir while the pump was rotating. The inlet and outlet ports of the pump were connected with straight tubes long enough to obtain a fully developed flow before and after the pump. The fluid temperature was also measured at each experiment.

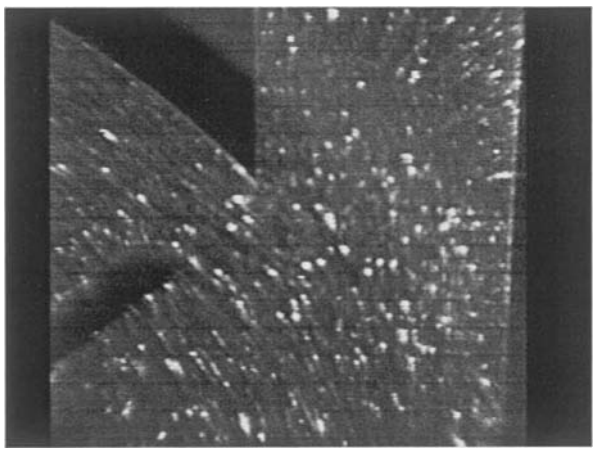

Fig. 4. A typical video image obtained throughout the experiments. The vane area shown here is analyzed in detail in Chap. 3.1.

2.4 Image Acquisition

A laser light sheet and a high speed video camera were used in the experiments. The laser light sheet (width: 1.6 mm) was generated by an Argon ion laser (7W capacity, LEXEL, Fremont, CA, USA) and a cylindrical lens. Images were taken with the black and white high speed video camera (256×256 pixel, 4500 full frame/s, FASTSCAM-ultima-UV, Photron Ltd., Tokyo, Japan) and were recorded on a video disc (LVR-3000AN, Sony, Tokyo, Japan). The speed of the video camera was selectable, to find the sufficient camera speed to detect the particle movement. The highest recording rate of the camera was 4500 frames/s in full frame mode, and in some cases a half frame mode with a speed of 9000 frames/s was used. After acquisition, images were transferred to the computer's memory, the image size was 512×480 pixel and image resolution varied between 30-200μm/pixel.

2.5 Image Analysis: PTV

Velocity vectors of the tracer particles were then analyzed by four frame particle tracking system (Current, Kanomax Ltd., Osaka, Japan) running on a NEC personal computer. The software is based on the theoretical background laid down in Kobayashi et al. (1991). The method was developed for measuring high velocity flow field, opposite to PIV techniques that can be applied to low velocity flow fields with high particle density.

In our case of high flow velocity and low particle density, the identification of each particle and its path gave better results. The applied four frame tracking was based on a search on the second frame in the vicinity of the particle position of the first frame. This process was repeated three times (Fig. 5). By finding the same particle on all four frames, the analysis of the relationship of the four position could reduce possible error by defining the allowable deviation of the path of a particle moving with a constant speed. As a high speed video camera was used and particles moved only 1-10 pixels between frames, this assumption could significantly reduce errors.

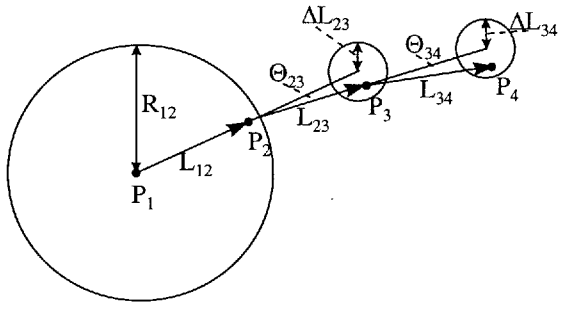

Fig. 5. Four frame particle tracking.

Particles were searched for, on the second frame, in the vicinity of the particle position of the first frame. Setting the search area specified the vector length and by finding the second position of the particle, the general direction of the particle movement was also determined. After this, the software searched for two more possible positions, and if particles were found in the searching area, the particle movement was determined.

Steps of the PTV analysis:

- Image acquisition. Digitizing the video image provided by the video disc recorder.
- Image enhancement.
- Binarization. For the separation of the noise (lower gray scale values) and signal (higher gray scale values). The original image was an 8 bit grayscale image which is transferred into a binary image. Setting the binarization threshold is important as one can reduce the number of error vectors. This has to be done manually or can be based on a history analysis of the grayscale image, as image quality differs from experiment to experiment.
- Area selection. Selecting the important area for analysis can reduce the processing time.
- Particle identification. Based on the binary image, the center of gravity is determined for each particle on the image. The search has an additional parameter for excluding too large size particles. This was in our analysis a size limit, for sizes larger than 30 pixel. This is necessary as the error in determining the particles' center of gravity position increases and also large particles many times results from overlapping particles.
- Particle tracking was done as explained earlier in this section.

2.6 Image Analysis: Post-processing

The resulting raw data, containing vector position, size and direction, were further processed by custom developed software (Borland C++ 4.5, Windows 95 platform) running on an IBM compatible personal computer. The post-processing consisted of the following steps:

- Error reduction based on the velocity distribution of the vectors. Vectors which did not follow the general flow field were eliminated.
- Moving surface extraction. Vectors which are moving together with the impeller surface are assumed to be produced by particles attached to the surface. Since these vectors, in some case, represent 20-70% of the total vectors, their extraction becomes necessary.
- Time frame extraction. In cases where data from many frames are superimposed, it becomes necessary to exclude certain intervals (vane pass, etc.).
- Transformation to rotating coordinate system. Viewing secondary flow patterns can reveal many important phenomena of the flow. Transformation can be necessary to the rotating coordinate system of the impeller or to a coordinate system moving together with the main flow.
- Superimposing many frames. From the nature of the PTV analysis, in certain cases the collected vector/frame ratio is very low, it can be as low as a few particles. For obtaining analyzable data, many of these frames should be superimposed and analyzed together. This analysis assumes that the flow is the same if the impeller position is the same. In one rotation, depending on the vane number, 4 to 6 frames can be collected. For certain analysis it is acceptable to superimpose frames regardless the impeller position. By this way a few thousand frames can be analyzed together.
- Grid point evaluation. The strength of the PTV method lays in the property that it shows actual particle vectors and path. In some cases, especially when the number of vectors is very large (superimposed frames), grid point averages of the velocities are useful. This feature enables the analysis of general flow behavior as well as shear analysis which is built on grid point description.
- Particle path. By taking approximately one thousand images in one series, following the path of every single particle is also possible. This analysis is possible only when the flow is nearly two dimensional and the laser light sheet is parallel with the flow direction.
- Velocity distribution analysis. Besides the general flow behavior which can be followed by the particle path, it becomes important to evaluate the actual velocity distribution in the flow field. A coloring method was developed which uses four colors to show the speed range from the slowest velocities to the higher velocities on the images. This can easily point out the areas of higher and lower velocity flow fields.
- Besides the analysis steps, user friendly sub-functions were built in the software, which enabled the presentation of the results in different formats, by using zoom, colors, re-sizing and scaling, adding text and graphical information.

In Chap. 3, we will show some applications for all the above mentioned post-processing steps and methods.

2.7 Error Analysis

The following errors occur during the flow visualization experiments. The methods for error reduction are also included. Errors not directly related to image analysis and PTV are not listed here (flow rate, rotational speed measurements, etc.). The first group consists of error sources before image acquisition:

- How well the particle follows fluid movement? To reduce the influence of this error source the specific gravity of tracer particle should be close or equal to that of the working fluid. Since the 0.15 mm tracer particles did not precipitate over 10 minutes as was mentioned, the traceability to flow was satisfactory.
- Distribution in particle sizes. Careful selection for the maker of particles is necessary.
- Width of laser sheet. Laser sheet should be as thin as possible since wide laser sheet would show 3D flow movement also.

Errors related to image acquisition and PTV analysis:

- Camera distortion, acrylic model distortion. To reduce this error, the camera has to be placed in a position perpendicular to the model. Model and working fluid refractive index have to be kept identical and constant.
- Center of gravity determination in PTV analysis:
  - screen coordinates are discrete (256×256, 512×480),
  - depending on the strength of the laser, particle sizes on the screen are different, with larger power they become larger sized,
  - the shape of the particle spot is not spherical.

To reduce this error, the vectors should be as long as possible. This can be achieved by correct parameter setting of the particle tracking.

- Non existing vectors, generated by the 4 frames method. By setting the parameters mentioned in Sec 2.7, this error can be minimized. For further minimization, vector length distribution is analyzed and vectors having deviant length can be excluded.

For the present experiment the screen is composed of 256×256 pixels and particles occupying 1 to 30 pixels can be found on an image. Particle images with different sizes and shapes cause approximately 1.5 pixel error, which causes 0.6% pixel error in a 256 pixel region and 10% velocity error for vectors of 15 pixels as a mean. Magnification of image by zooming or elongation of vectors by skipping frames would be useful. Image of boundary includes 3 pixel (1.2%) errors in a 256 pixel region due to unsharpness mainly caused by observed area thickness. Sheet laser thickness, 1.6mm, causes 4.2% velocity errors at 50% or 37.5 mm radius (as a mean). Since 0.15 mm-dia particles were used, velocity data are lacking in the 0.075 mm vicinity of the walls. The particles have a data-smoothing effect for a ±0.075 mm region.

3. Applications

In this section we present a few applications of the post-processing methods described in Chap. 2.7. We also mention the biological/medical application of the results, but detailed analysis can be found in previous works: Ikeda et al. (1996), Nishida et al. (1997), Yamane et al. (1998), Asztalos et al. (1999). The methods are separated into two groups based on their aim, gathering the know-how for shear analysis (Chap. 3.1) and for analyzing the recirculating flow (Chap. 3.2) which has a high potential in artificial heart research as prevention of hemolysis or thrombus from the pumps.

3.1 Shear Evaluation

The evaluation of shear and its location in the blood pumps is of primary importance. Shear is directly linked to hemolysis, which should be minimized for artificial heart usage. By analyzing the locations of the highest shear the engineering design for reducing hemolysis becomes straightforward.

Comparison between flow fields in the diffuser area

Models 3 and 4 were made to evaluate pump designs. Flow pattern was evaluated in the diffuser area in order to compare models with standard radial gap and with small radial gap (Fig. 6.). As expected, the gap size had a large effect on the flow in the outlet. Impeller outflow smoothly entered the straight diffuser for the standard gap size model. In contrast, the outflow for the small gap size model moved toward the inner wall of the diffuser forming a high speed jet and it was accompanied by a low speed stagnant region in the vicinity of the outer wall. By using color coding for different speed it becomes possible not only to see the direction of the flow, but also to see the size distribution.

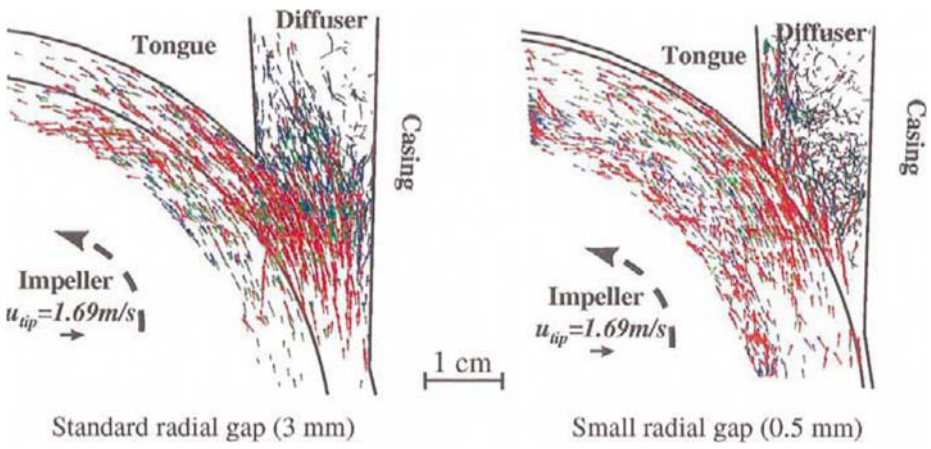

Fig. 6. Comparison between Model 3 and Model 4 in the outlet region. Absolute vectors show clear differences between the two models. Color denotes speed in the pumps. High rotational speed condition (259 rpm). (black: 0<v<0.77m/s, blue: 0.77m/s<v<0.95m/s, green:0.95m/s<v<1.1m/s, red: 1.1m/s<v)

Shear location evaluation in the diffuser area

When position and velocity in a two dimensional region are mostly in the plane of observation, evaluation of two dimensional shear distribution is possible. Shear velocity is defined by:

$$\partial u/\partial y + \partial v/\partial x \qquad (1)$$

where u, v are the x, y components of the velocity vector. First, grid point vectors are calculated on the data presented on Fig. 6. Based on the grid vectors and (1), shear velocities were calculated. The results are shown on Fig. 7. For both configurations high shear spots can be found at both sides of the diffuser close to the solid wall. Higher shear and wider high shear area was found in the case of Model 4 with small radial gap. The high shear areas were the tongue of the diffuser and the outer wall area where the diffuser bifurcates from the volute. As it can be seen, the highest shear values are close to 1400 s^{-1} in the experimental model, which is 1400 $s^{-1} \times 10.4$ = 14560 s^{-1} in the case of the real size pump model. This high shear is expected to be directly related to hemolysis and, therefore, these results were compared to hemolysis tests. Results showed high similarity with finding higher level of hemolysis in the case of the small gap model. This emphasizes the importance of the radial gap size, as a rule of thumb it should be large enough to keep the hemolysis level low. Also small gap distorted 0velocity profile in the diffuser area (Fig. 6), which decreased the pump head, therefore reduced the efficiency of the pump.

Quantitative shear analysis in the vane and freeflow area

The combination of different analysis methods is presented to obtain a complete picture of the flow in the vane area of Model 2. The flow entering through the inlet moves into the closed-type impeller then spreads out into the volute area driven by the vanes. Flow has a high speed in this region, therefore hemolysis is expected to occur. Besides the flow patterns, obtaining the highest value of shear in the region was also the purpose of this experiment.

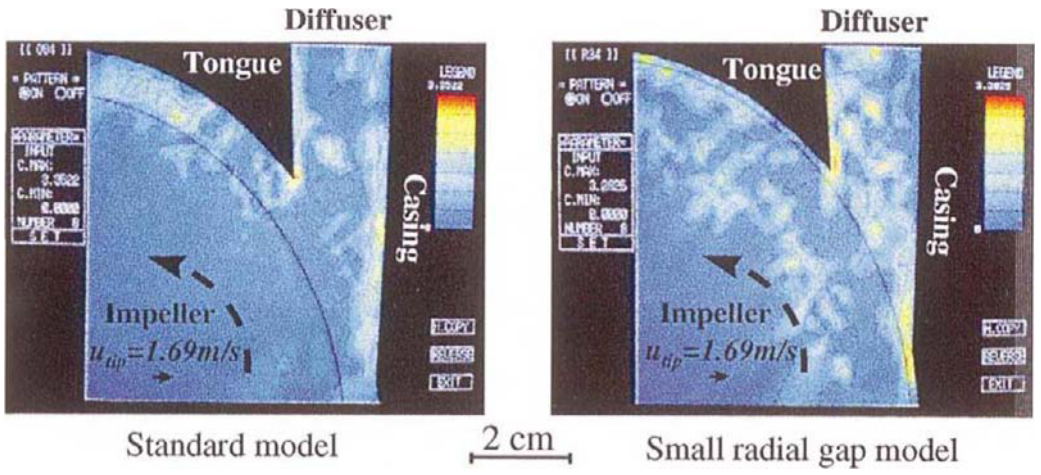

Fig. 7. Shear distribution of Model 3 and Model 4. Grid point averages of Fig. 6 were used to calculate the shear distribution in the outlet region. High rotational speed condition (259 rpm). The top of the scale (red) is 1400 s^{-1} for the experimental model which is 14560 s^{-1} (see text) for the real size model.

(a)

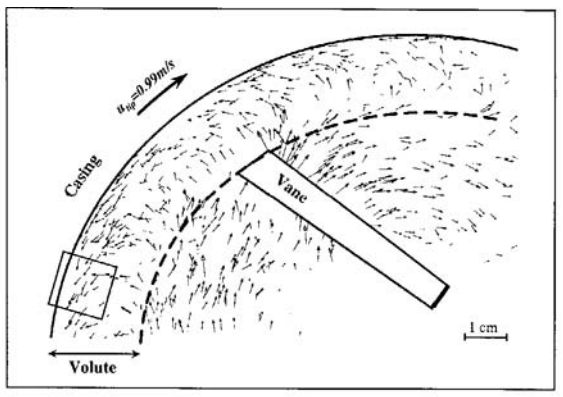

(b)

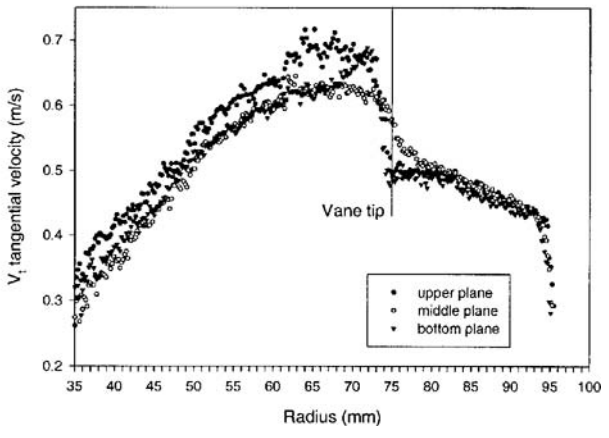

Fig. 8. Flow in the vane area of Model 2.
(a) Flow is shown in a relative coordinate system, which was moving with half impeller speed. The reference speed is selected, as an approximation of the core velocity, to produce the most effective visualization of the phenomena in question. Figure clearly shows the separation behind the tip of the vane, and that the flow slows down near the casing wall.
(b) The velocity profile of the same area is shown where a large velocity drop can be seen at the vane tip (separation) and near the volute wall. Three curves present the three investigated layers with each point representing average tangential velocity.

Analyzing Fig. 8, one can clearly see two large speed drop areas, at the vane tip, and at the casing wall. Fig. 8a shows a cross-section in the middle between the front and back shroud, while on Fig. 8b, data from three layers can be seen, with layers close to both the front and back shroud of the closed type impeller, and the layer in the middle section. The speed drop is especially large next to the rotating shrouds, where the centrifugal effect drives the flow among the vanes, and the drop occurs because this driving force disappears.

The other large drop occurs in the vicinity of the casing wall. This region is very small, therefore one expects a high shear to be located mostly in this area. Close-up view was utilized to analyze the flow and is shown on Fig. 9. Shear velocity was calculated by quantitative analysis of Fig. 9b. For the scale-up model, evaluated shear near the volute wall ranges between 573 s^{-1} and 1290 s^{-1} and is in the 0.6 mm vicinity of the solid surface. Based on the similarity law, the highest shear in the actual size pump is predicted to range between 8600 s^{-1} and 19400 s^{-1} and is located in the 0.2 mm vicinity. This value represents the highest shear expected in the pump, and red blood cells are exposed to this shear only for a short time because of the high rotational speed. The wide range of the maximum shear value is given, as the shear increases with the vane passing nearby, giving periodic character to the flow patterns. From Fig. 9b, one acknowledges the necessity of the deceleration region between the vanes and the volute wall to reduce the size of the high shear region.

(a)

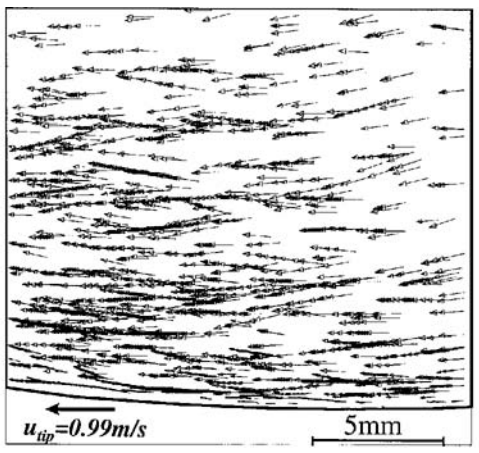

(b)

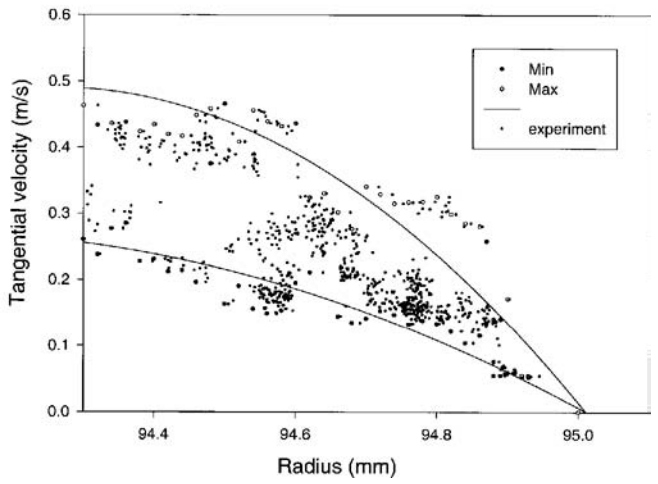

Fig.9. Close-up view of the area denoted on Fig. 8a. Shear velocity is calculated by the bounding curves fitted on the data (b) obtained from the vector map (a).

3.2 Analysis of Flow Recirculation

Thrombus formation or blood clotting should be investigated and completely eliminated. Its primary cause can be found in the effect of stagnation. Low fluid motions, stagnating and trapped fluid should be identified and eliminated. The areas where this could occur are mostly the gap regions in the pumps. The flow analysis in the gaps reveals the recirculation of the fluid entering the gaps. Gaps include the front gap and back gap, having flow returning to the inlet and flow returning to the main flow through the washout holes respectively.

Evaluation of the absolute velocity field in the inlet

Flow entering the inlet region of Model 2 (Fig. 10a), changes its velocity profile along the axis of the inlet. For the visualization of this phenomenon, showing unprocessed velocity data seems to be the most convenient. This data, without much further processing, describes well the underlying phenomena. Still the use of this expression is limited in areas where the flow field consists of a main flow and a secondary flow superimposed on it. Also very large number of vectors can result in not clear understanding.

(a)

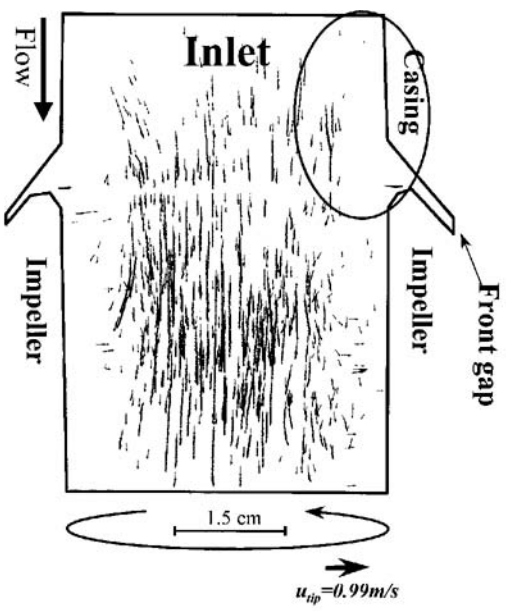

(b)

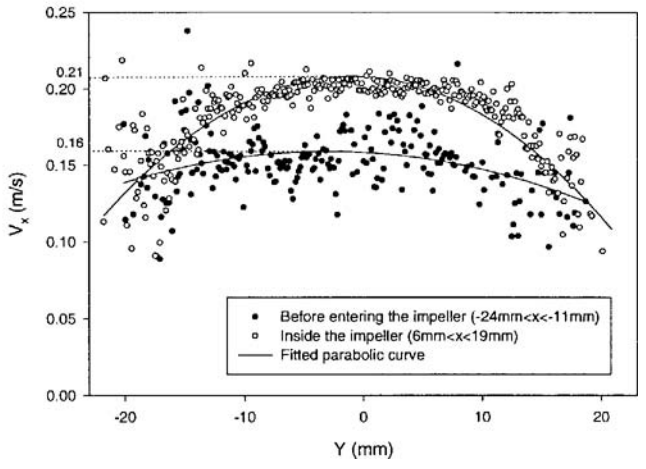

Fig. 10. Flow entering the inlet of Model 2.
(a) Absolute velocities seen in the 3× scale-up model.
(b) Velocity profiles seen before and after the inlet edge of the rotating impeller.

By analyzing Fig. 10a one concludes the following. The flow starts rotation upon entering the impeller, and flow returns from the front gap of the pump. This returning flow has a high rotational component, therefore its visualization carries more difficulty compared to the relatively smooth flow entering the main inlet area. The returning jet induces turbulence, disturbing the main flow. The effect of centrifugal force can be seen close to the rotating impeller wall.

Velocity profiles, before and after the inlet edge of the impeller, are compared on Fig. 10b. This figure gives all the velocity data. By calculating the flow rate change before and after the front-gap-flow enters the main flow (using area integral and assuming parabolic flow profile), the flow rate in the front gap was found to be 30% of the flow rate of the external circuit (9L/min), which coincides well with area-weighted moving averaged velocity calculations. This result shows sufficient washout in the front gap.

Grid point evaluation in the inlet

As it was mentioned earlier, flow returning from the front gap of Model 2 to the inlet region carries certain difficulty to analyze. Therefore different analysis parameters and a more closer view of the pump were used. Due to the very large number of resulting vectors, showing all vectors could not give a clear picture of the flow characteristics. Grid point averaging was used to reduce the amount of data, and the result is shown on Fig. 11. Besides reducing the amount of data, grid point evaluation has the feature of reducing error, by its averaging property. Flow returning from the impeller-casing gap can clearly be seen. After entering the main flow channel, this flow is driven along the surface against the main flow, and causing vortex formation when eventually turning back. Since particles close to the rotating impeller were not identified as their velocity is mainly perpendicular to the observation plane, they do not stay long enough in the laser light sheet to be recognized by the four frame tracking method.

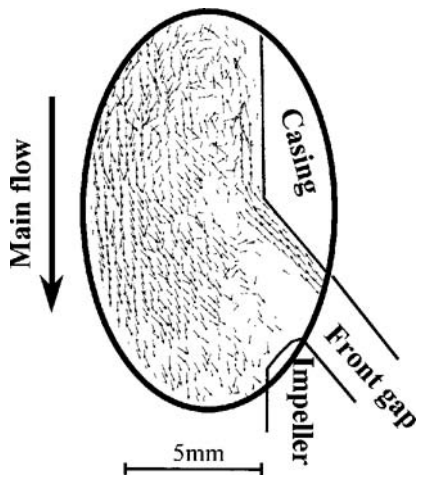

Fig. 11. Enlarged area of Fig. 10a. Flow returning from the front gap of the impeller is shown in grid point averages.

Relative velocity field around the washout hole

Flow returns from the back gap to the main flow through the washout holes. In Model 2 washout holes were introduced to prevent thrombus by recirculate the stagnant blood in the back gap area of the impeller. Visualization results of this region can show the vortex formation if the particles are viewed from a coordinate system fixed to the moving impeller. From this moving frame, flow around the entrance of the washout hole is shown on Fig. 12. As there are areas with spiral vortices in the rotational direction, the actual fluid movement occurs with higher speed than the actual impeller speed at that point. This signals the importance of flow patterns in this area. Vortices are formed before entering the washout hole. To avoid possible flow separation around the entrance it is important to manufacture a smooth entrance, eliminating the sharp edges.

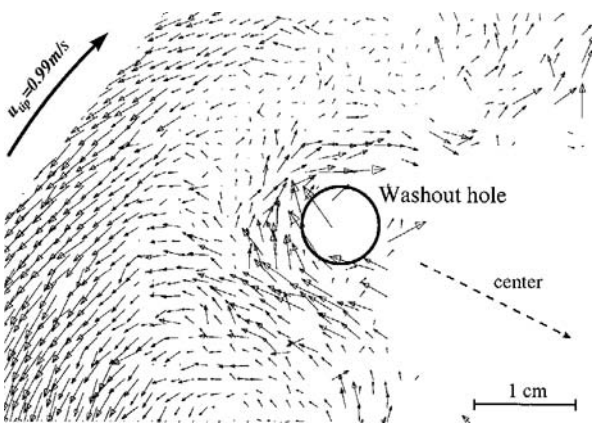

Fig. 12. The vicinity of the washout hole of Model 2. All vectors are shown in a relative coordinate system fixed to the moving impeller, expressed by a grid point averaging.

Particle path around the washout hole

A similar region as in section was investigated in Model 1. The purpose was to see particle movements, particle path before entering the washout hole. It was necessary also in this experiment to transform the resulting data to a moving coordinate system. Fig. 13 shows the particles spiraling into the washout hole.

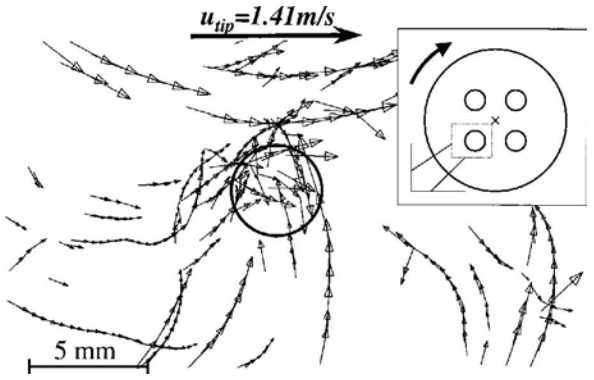

Fig. 13. The vicinity of the washout hole of Model 1. Particle paths are shown in a rotating coordinate system, which rotates together with the impeller.

4. Concluding Remarks

A centrifugal blood pump for artificial heart has to have low hemolysis and no thrombus formation. For finding and removing the fluid dynamic causes of the above mentioned phenomena, flow visualization was utilized, as flow visualization can identify the high shear and stagnation locations which relate to hemolysis and thrombus formation respectively. In the present paper, general fluid dynamic characteristics of centrifugal blood pumps were extracted, through analyzing four typical centrifugal pumps with flow visualization technique. Finding shear velocities in the volute and diffuser regions, confirming vortex formation at washout holes, and quantitative analysis of the flow in the inlet regions were the shown as examples. All these phenomena are typical and common to all the centrifugal blood pumps. The results also showed the way of reducing high shear by larger radial gaps and by smooth manufacturing of edges. The obtained results correspond well to hemolysis tests, which proves that flow visualization is a useful tool in developing and analyzing blood pumps for artificial hearts.

References

Asztalos, B., Yamane, T.and Nishida, M., Flow visualization analysis for evaluation of shear and recirculation in a new closed-type, mono-pivod centrifugal blood pump, to appear in Artificial Organs 1999., 23 (10):939-946.

Ikeda, T., Yamane, T., Orita, T. and Tateishi, T., A quantitative visualization study of flow in a scaled-up model of a centrifugal blood pump, Artificial Organs, 20-2 (1996), 132-138.

Kobayashi, T., Saga, T., Haeno, T. and Tsuda, N., Development of a real-time velocity measurement system for high reynolds fluid flow using a digital image processing design, Experimental and Numerical Flow Visualization ASME, 128(1991), 9-14.

Nishida, M., Yamane, T., Orita, T., Asztalos, B. and Clarke, H., Quantitative visualization of flow through a centrifugal blood pump: Effect of washout holes, Artificial Organs, 21-7 (1997), 720-729.

Yamane, T., Ikeda, T., Orita, T., Tsutsui, T. and Jikuya, T., Design of a centrifugal blood pump with magnetic suspension, Artificial Organs, 19-7 (1995), 625-630.

Yamane, T., Nishida, M., Asztalos, B., Tsutsui, T. and Jikuya, T., Fluid dynamic characteristics of monopivot magnetic suspension blood pumps, ASAIO Journal, 43-5 (1997/1), 635-638.

Yamane, T., Nishida, M., Kijima, T. and Maekawa, J., New mechanism to reduce the size of the monopivot magnetic suspension blood pump: direct drive mechanism, Artificial Organs, 21-7 (1997/2), 620-624.

Yamane, T., Asztalos, B., Nishida, M., Masuzawa, T., Takiura, K., Taenaka, Y., Konishi, Y., Miyazoe, Y. and Ito, K., Flow visualization as a complementary tool to hemolysis testing in the development of centrifugal blood pumps, Artificial Organs, 22-5 (1998), 375-380.

Author Profile

Balazs Asztalos: He received M.Sc. (Eng) degree in Electrical Engineering in 1993 from the Technical University of Budapest, and Ph.D in 1998 from the Hungarian Academy of Sciences in biomedical engineering. He has worked at Griffith University, Rotary Center for Cardiovascular Research, Australia on ultrasound ecocardiographic image analysis, and on artificial heart research at the Mechanical Engineering Laboratory, Japan. His research interests are image processing, biomedical control, artificial heart.

Takashi Yamane: He is Head of Biomimetics Division, Mechanical Engineering Laboratory, Japan. He received B.E. (1975), M.E.(1977) and Ph.D(1980) in Aeronautics from University of Tokyo. Finishing the research on Turbomachinery, he has been engaged in research and development of artificial heart since 1991.

Masahiro Nishida: He is Researcher of Biomimetics Division, Mechanical Engineering Laboratory, Japan. He received B.E. (1989), M.E.(1991) and Ph.D(1995) in Biomedical Engineering from Keio University. He has been engaged in research and development of artificial heart since 1995.

Toru Masuzawa: He is an Associate Professor of Mechanical Engineering at Ibaraki University, Hitachi, Japan. He received the B.S.(1982), M.S.(1984), and Ph.D(1991) degrees in applied system engineering, from Tokyo Denki University, Tokyo, Japan. He has been engaged in research and development of artificial heart since 1990.

Yoshiaki Konishi: He is project manager of R&D Division, Nikkiso Co.,LTD., and Consulting Engineer registered by STA Japan. He received B.S.(1972) in theoretical physics from Hirosaki University. He has been engaged in research and development of special pumps mainly for artificial heart.